LU-TP 23-06
May 2023

Glauber Monte Carlo for proton-proton and virtual-photon-proton collisions

Oscar Sepp

Department of Physics, Lund University

Bachelor thesis supervised by Christian Bierlich and Leif Gellersen

LUND
UNIVERSITY

Abstract

In high energy physics, we want to probe the inner structures and behaviours of the particles that are the building blocks of our universe. This is often done by colliding nuclei together. This bachelor thesis presents an implementation of a Glauber Monte Carlo simulation framework to determine the geometric quantities such as the number of participating nucleons N_{part} and the number of sub-collisions N_{coll} as well as the total and elastic integrated cross sections in high-energy collisions. The models include the black and grey disk models for proton-ion collisions and a dipole model for virtual-photon-ion collisions, which are fit to cross section data. The models rely on the optical theorem and Good-Walker formalism to calculate N_{coll} and N_{part} based on the impact parameter b. These models for proton-proton and virtual-photon-proton (γ^*p) collisions were found to be somewhat consistent with predicting the integrated total cross section as functions of the center of mass energy $\sqrt{s}$ (or virtuality Q^2 and center of mass energy W^2 in virtual-photon-proton γ^*p) whilst struggling with predicting the integrated elastic cross section for proton-proton collisions.

Populärvetenskaplig sammanfattning

Partikelkollisioner gör det möjligt för oss att studera de inre strukturerna och beteendena hos partiklar som utgör universum. År 1969 upptäckte forskare att protoner faktiskt består av mindre partiklar som kallas kvarkar genom kollisioner mellan elektroner och protoner. Så genom att kollidera partiklar så får vi ut hur dessa partiklar påverkar varandra men också som i fallet för protonen, vad de består av. När två högenergi partiklar kolliderar frontalt, upptäcks tusentals partiklar i detektorer som ALICE i The Large Hadron Collider (LHC). Andelen av de laddade partiklarna som detekteras beror på hur central kollisionen var mellan de två ingående partiklarna. Denna andel är proportionelig mot antalet deltagande partiklar i kollisionen N_{part} i en Glauber Monte Carlo simulering. Glauber Monte Carlo simulering kan även användar för att beräkna antalet delkollisioner (N_{coll}) i en kollision. Detta görs genom att en partikel är stationär (målet) och den andra i rörelse (projektilen).

Även om befintliga program som PYTHIA och HERWIG kan modellera dessa kollisioner, kommer det arbete som utförs här att från grunden se om resultaten kan jämföras med data och befintliga program. De specifika modeller som används här är två modeller för proton-jon kollisioner vilket inkluderar en svart och en grå disk modell och för virtuell-foton-jon kollisioner använder vi dipolmodellen. Svart och grå disk modellerna simulerar protonen som en tvådimensionell disk med radie R, och när två diskar överlappar med varandra har de kolliderat. Den grå disken har också en opacitet, det vill säga även om de två protonerna överlappar med varandra, beroende på hur opak vi gör protonen, dessto större sannolikhet för protonerna att kollidera. Dipolmodellen simulerar virtuella-fotononer och protoner som dipoler (ex. två kvarkar som är sammankopplade). Beroende på energin i kollisionen kan sedan dipoler utvecklas till nya dipoler vilket skapar en kedja av dipoler. Dipolerna anses sen vara kolliderade beroende på orienteringen och längden på dipolerna men också distansen mellan dem.

Contents

1 Introduction

In high energy physics, we want to probe the inner structures and behaviours of the particles that are the building blocks of our universe. For example the proton was thought of as a fundamental particle. But in 1969 at the Stanford Linear Accelerator Center (SLAC) through deep-inelastic scattering in electron-proton collisions [1], it was discovered that the proton was actually comprised of smaller point-like particles which we now call quarks.

In general, when we collide two high energy particles head on in a particle collider, for example two nuclei, the number of particles that get detected in the detector will be in the thousands as a result of the collision. We know that for a nucleus, it consists of protons and neutrons. So we might ask, how many of these protons and neutrons where participating in the collision (N_{part})? How many sub-collisions where there (N_{coll}) and how does this depend on the centrality of the collision? These geometric quantities are something that a Glauber Monte Carlo simulation tries to determine. Although N_{part} and N_{coll} cannot be measured directly in a particle collider, they can be mapped to other quantities that can be measured (however this will not be done here). For example the number of participating nucleons is proportional to the number of detected charged tracks in the detector.

There are a couple of ways of implementing a Glauber Monte Carlo and some frameworks already exists like PYTHIA [2] and HERWIG [3]. In these frameworks there exists models for each type of collision with different parameters fit to match data. The question now arises, why are we making another framework if there already exists more than one? One reason is to gather all of the building blocks of what is needed to make a working Glauber Monte Carlo and see if the results can compare to data and the other frameworks.

In sections 2 and 3 some models for proton-proton (pp) and virtual-photon-proton (γ^*p) collisions will be introduced. The models are then fit to cross section data and then used to calculate the geometric quantities N_{coll} and N_{part} depending on the impact parameter b. The type of models that are discussed here will rely on the optical theorem and Good-Walker formalism (see section 2). These models are the black and grey disk models for proton-ion collisions which model the nucleons as a disk of radius R, and a dipole model for virtual-photon-ion collisions which models the virtual photon and the ion as a collection of dipoles. The parameters of the models are then fitted towards data of total integrated cross sections for the specific collision and used for calculating N_{part} for virtual-photon-ion and proton-ion collisions.

2 Theory

In this section we introduce the theoretical building blocks for a Glauber Monte Carlo which are used in the following sections for estimating total and elastic cross sections for different types of collision models.

2.1 Optical theorem

In a scattering process of an initial state going to a final state, the imaginary part of the elastic amplitude A_{el}, with $|A_{\text{el}}|^2$ being the probability of having an elastic scattering, is given by the optical theorem which in a convenient from can be written as [4]

$$\text{Im}(A_{\text{el}}) = \frac{1}{2}\bigg(|A_{\text{el}}|^2 + \sum_j |A_j|^2\bigg), \tag{2.1}$$

where the sum runs over all inelastic channels j. Note that the right hand side is the total cross section divided by two. The real part of the elastic amplitude diminishes as the energy of the collision increases [4]. This means that we can write for high enough energies, $A_{\text{el}} = i\,\text{Im}(A_{\text{el}})$. Using this, Eq. (2.1) can be rewritten as

$$-iA_{\text{el}} = \frac{1}{2}\bigg(-A_{\text{el}}^2 + \sum_j |A_j|^2\bigg), \tag{2.2}$$

$$\implies A_{\text{el}} = i\bigg(1 - \sqrt{1 - \sum_j |A_j|^2}\bigg). \tag{2.3}$$

And in impact parameter space

$$A_{\text{el}}(\mathbf{b}) = i\bigg(1 - \sqrt{1 - P_{abs}(\mathbf{b})}\bigg), \tag{2.4}$$

where $P_{\text{abs}} = \sum_j |A_j|^2$ is the probability for absorption into inelastic channels and $\mathbf{b}$ is the impact parameter.

2.2 Good-Walker formalism and cross sections

We now consider the interaction between two objects which we will call target and projectile. This interaction can be considered in the Good-Walker formalism which introduces two wave functions $|\Psi_I\rangle$ and $|\Psi_S\rangle$ which are the initial state (before the interaction) and the final state of the system (after the interaction) with a complete set of normalized eigenstates $\{|\psi_i\rangle\}$ of the scattering amplitude $\hat{T}(\mathbf{b})$. $|\Psi_I\rangle$ and $|\Psi_S\rangle$ are related by $|\Psi_S\rangle = \hat{T}(\mathbf{b})\,|\Psi_I\rangle$, where $\hat{T}(\mathbf{b}) = -iA_{\text{el}}$ [4] (also related to the $\hat{S}$-matrix by $\hat{T} = 1 - \hat{S}$), with eigenvalues $\hat{T}(\mathbf{b})\,|\psi_i\rangle = T_i(\mathbf{b})\,|\psi_i\rangle$. We now look at a interaction between a target and a projectile in an A+B collision. The incoming wave function $|\Psi_I\rangle$ can be written as an expansion in the basis $|\psi_i\rangle$ as

$$|\Psi_I\rangle = \sum_{p=1}^{N_p}\sum_{t=1}^{N_t} c_p c_t\,|\psi_p, \psi_t\rangle \equiv \sum_{p,t} c_p c_t\,|\psi_{p,t}\rangle\,, \tag{2.5}$$

where N_i is the number of nucleons in nuclei i and c_i are the expansion coefficients for $i = p, t$. The scattered wave function $|\Psi_S\rangle$ (outgoing wave function) is related to the incoming wave function by

$$|\Psi_S\rangle = \hat{T}(\mathbf{b})\,|\Psi_I\rangle = \sum_{p,t} c_p c_t T_{p,t}(\mathbf{b})\,|\psi_{p,t}\rangle\,. \tag{2.6}$$

The overlap between Eqs. (2.5) and (2.6) is then

$$\langle\Psi_I|\Psi_S\rangle = \langle\Psi_I|\,\hat{T}(\mathbf{b})\,|\Psi_I\rangle = \sum_{p,t} |c_p|^2 |c_t|^2 T_{p,t}(\mathbf{b}) \tag{2.7}$$

$$\equiv \langle T(\mathbf{b})\rangle_{p,t}\,, \tag{2.8}$$

where $\langle T(\mathbf{b})\rangle_{p,t}$ is the probability amplitude of an elastic scattering. The elastic cross section $\sigma_{\rm el}$ is then

$$\frac{d\sigma_{\rm el}}{d^2b} = \langle T(\mathbf{b})\rangle_{p,t}^2\,. \tag{2.9}$$

The total cross section follows directly from the optical theorem (2.1) since the right hand side is the total probability for a scattering to happen

$$\frac{d\sigma_{\rm tot}}{d^2b} = 2\,\langle T(\mathbf{b})\rangle_{p,t}\,. \tag{2.10}$$

The integrated cross sections are then given by integrating equations (2.9) and (2.10)

$$\sigma_{\rm el} = \int d^2b\ \langle T(\mathbf{b})\rangle_{p,t}^2\,, \tag{2.11}$$

$$\sigma_{\rm tot} = \int d^2b\, 2\,\langle T(\mathbf{b})\rangle_{p,t}\,. \tag{2.12}$$

2.3 Dipole-dipole model for virtual-photon-proton collisions

We now move into a virtual-photon-proton collision model where the virtual-photon is the projectile that hits the stationary target proton. In the simplest case we see the virtual-photon splitting into a quark-antiquark ($q\bar{q}$) dipole with the size of the dipole $r \propto 1/Q$, where Q is the virtuality of the virtual-photon (see fig. 1). This dipole then interacts with the target proton which we will approximate as three quarks in an equilateral triangle with the distance between each dipole $r_{\rm p} = 1/(3m_{\rm p})$ where $m_{\rm p}$ is the mass of the proton. The leading interaction between two quarks is an exchange of a single gluon, and hence for a dipole-dipole interaction, the largest contribution comes via two gluons, which will then create two new dipoles as in figure 2. The cross section in impact parameter space $\sigma_{\rm dip}$ for this dipole-dipole interaction is [5]:

$$\frac{{\rm d}\sigma_{\rm dip}}{{\rm d}^2b} = \frac{\alpha_s^2}{2}\log^2\left(\frac{r_{13}r_{24}}{r_{14}r_{23}}\right) \equiv f_{ij}, \tag{2.13}$$

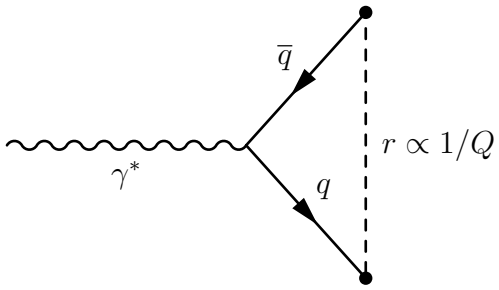

Figure 1: A visualisation (not a Feynman diagram) of a virtual-photon evolving into a $\bar{q}q$ dipole with the size of the dipole $r \propto 1/Q$.

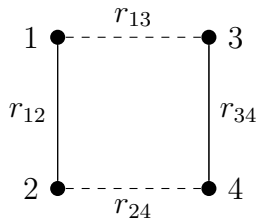

Figure 2: Visualization of a dipole-dipole collision where the original dipoles (filled lines) interact with each other to create two new dipoles (dashed lines).

where α_s is the strong coupling constant and r_{nk} where $n = 1, 2$, $k = 3, 4$ are the distances between the nodes of the dipoles n and k. f_{ij} is then defined as above for each dipole i and j for the projectiles and targets respectively (we will later evolve the projectile in rapidity to branch out into dipole chain). This f_{ij} can be thought of as an indicator of how likely two dipoles are to have an inelastic collision (note: f_{ij} is not between 0 and 1 and hence not a probability). Now assuming that each dipole collision ij is independent of each other, we can now write the scattering amplitude $T(\mathbf{b})$ for the dipole-dipole collision as [4]

$$T(\mathbf{b}) = 1 - \exp\bigg(-\sum_{ij} f_{ij}\bigg), \tag{2.14}$$

where we sum over all dipole-dipole interactions.

Going back to our original model of our virtual-photon branching into a quark-antiquark pair $|\gamma^*\rangle \to |\bar{q}q\rangle$, we instead allow it to branch out (i.e $|\gamma^*\rangle \to a_1 |\bar{q}q\rangle + a_2 |\bar{q}gq\rangle + a_3 |\bar{q}q\bar{q}q\rangle + \dots$) where $|a_i|^2$ is the probability for γ^* to branch into the i:th state. The probability P of a dipole i spanned by the coordinates $\mathbf{r_1}$ and $\mathbf{r_2}$ with the distance between them r_{12} to branch into a new dipole r_{23} is given by the evolution equation [5]

$$\frac{\mathrm{d}P}{\mathrm{d}y} = \mathrm{d}^2\mathbf{r_3}\frac{N_c\alpha_s}{2\pi^2}\frac{r_{12}^2}{r_{13}^2 r_{23}^2}, \tag{2.15}$$

where y is the rapidity which for γ^*p is $y = \log(W/m_\mathrm{p})$ where $W^2 = Q^2(1-x)/x + m_p^2$ is the center of mass energy and x is the Bjorken x.

3 Implementation

The following section introduces the methods used to compute the cross sections for virtual-photon-proton, proton-proton, and proton-ion collisions.

3.1 Woods-Saxon distribution

The sampling of the nucleons inside the nucleus is done according to the Woods-Saxon (WS) distribution [6]

$$\frac{\rho(\mathbf{r})}{\rho_0} = \frac{1}{1 + \exp\left(\frac{r-R}{a}\right)}, \tag{3.16}$$

where $\rho(\mathbf{r})$ is the density of nucleons at position $\mathbf{r}$ ($r = |\mathbf{r}|$), ρ_0 is the density at the center, $R = 1.1A^{1/3} - 0.656A^{-1/3}$ fm is the nuclear radius (A being the number of nucleons in the nucleus) and $a = 0.459$ [6] fm is the skin depth. To not have nucleons overlapping, we will introduce a hard core repulsion with $d = 0.9$ fm [6] (protons must be a minimum of 0.9 fm from each other center to center). Each nucleon of the nucleus will be placed according to the distribution $4\pi r^2\rho(r)$ since if we have a sphere $V = 4\pi r^3/3$, the probability to randomly sample a volume element is $dV = 4\pi r^2 dr$. The distribution we then want to sample from is then $4\pi r^2\rho(r)$.

The sampling of the nucleus on the computer is done by a hit and miss Monte Carlo approach using a box. We start by picking a uniform random number for the coordinates of a nucleon x, y, z in a reasonable range. We will use the range $-R < (x, y, z) < R$ but the larger the range, the more accurate at the edges and time consuming the nucleus generation will become. The radius r and $\rho(r)/\rho_0$ is then calculated, after which a uniform random number $X \in [0, 1]$ is generated. If $\rho(r)/\rho_0 < X$, the nucleon is rejected and a new coordinate (x, y, z) and X is generated. If it is accepted, we now check that the distance between it and all other generated nucleons is less than the hard core repulsion d (i.e if it overlaps with another nucleon). If it overlaps we go back to generating new coordinates and if it doesn't we accept it. This process is then repeated until the number of nucleons generated are the same as the number of nucleons desired A.

3.2 Impact-parameter sampling

The impact parameter $\mathbf{b} = (b, \varphi)$, being the projectiles' offset from the target in polar coordinates (see figure 3), is sampled from the distribution $2\pi b$ ($0 < b < b_{\max}$) for the same reason as in section 3.1 with $V \to A = \pi r^2$. The sampling for b is done by the inverse transform sampling method with $f(b) = 2\pi b$, i.e. we want to find the inverse of the primitive function $F(b)$, $F^{-1}(b)$. Starting with the primitive function

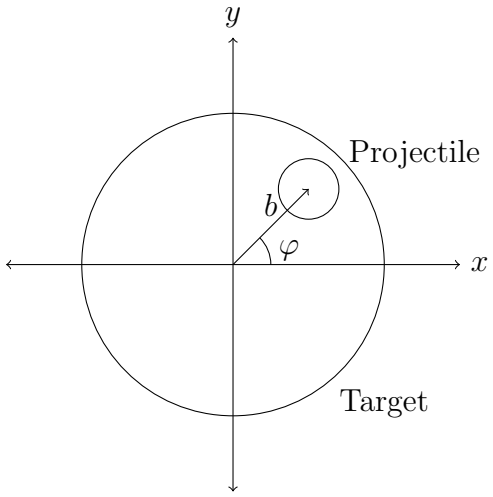

Figure 3: Visualtisation of a target (large circle) and a projectile (small circle) in the xy plane with the projectile going the the z direction.

$$F(b) = \int_0^b f(b')\,db' = X\int_0^{b_{\max}} 2\pi b'\,db', \tag{3.17}$$

$$= X\pi b_{\max}^2, \tag{3.18}$$

where $X \in [0,1]$ is a uniform random number and $b_{\max}$ is the maximum value of b. $b_{\max}$ is chosen to be just large enough to cover the whole nucleus. Also note that $F(b) = \int_0^b 2\pi b'\,db' = \pi b^2$ and plugging in $F^{-1}(x)$ into $F(b)$, we find

$$b = F(F^{-1}(b)) = \pi(F^{-1}(b))^2, \tag{3.19}$$

$$\implies F^{-1}(b) = \sqrt{\frac{b}{\pi}}. \tag{3.20}$$

This together with Eq. (3.18) gives us the equation from which b is sampled from

$$b = F^{-1}(F(b)) = F^{-1}(X\pi b_{\max}^2) = \sqrt{Xb_{\max}^2}. \tag{3.21}$$

The angular position φ of the impact parameter is sampled as $\varphi = X2\pi$ where $X \in [0,1]$ is a uniform random number.

3.3 Proton-proton collision models

Using Eq. (3.21) and a predetermined scattering function $T(b)$, we can calculate the cross section using equations (2.11) and (2.12). Starting with the black disk model, we let the

scattering amplitude $T(b)^{\text{bDisk}} = \Theta(R-b)$ where $\Theta(R-b)$ is the Heaviside step function and R is the radius of the disk (target). The analytical solution for the total cross section is

$$\sigma_{\text{tot}}^{\text{bDisk}} = \int d^2b\, 2T(b) = \int_0^{2\pi} d\varphi \int_0^{\infty} db\, 2\Theta(R_{\text{b}} - b)b, \tag{3.22}$$

$$= 2\pi R_{\text{b}}^2, \tag{3.23}$$

where R_{b} is the radius of the black disk. And the elastic cross section

$$\sigma_{\text{el}}^{\text{bDisk}} = \int d^2b\, T(b)^2 = \int_0^{2\pi} d\varphi \int_0^{\infty} db\, \Theta(R_{\text{b}} - b)^2 b, \tag{3.24}$$

$$= \pi R_{\text{b}}^2. \tag{3.25}$$

The grey disk model introduces some opacity α ($0 < \alpha < 1$) to the disk and the scattering amplitude is then given by $T(b)^{\text{gDisk}} = \alpha\Theta(R_{\text{g}} - b)$ where R_{g} is the radius of the grey disk. Its analytical solutions for the integrated cross sections are

$$\sigma_{\text{tot}}^{\text{gDisk}} = 2\pi\alpha R_{\text{g}}^2, \tag{3.26}$$

$$\sigma_{\text{el}}^{\text{gDisk}} = \pi\alpha^2 R_{\text{g}}^2. \tag{3.27}$$

From experimental results $\sigma_{\text{el}} \approx \sigma_{\text{tot}}/4$ at high energies [7, 8]. This implies for the grey disk model that the opacity $\alpha = 1/2$. To keep the total cross section the same for both the grey disk and black disk model, the radius of the grey disk R_{g} must be modified by

$$\sigma_{\text{tot}}^{\text{gDisk}} = \sigma_{\text{tot}}^{\text{bDisk}}, \tag{3.28}$$

$$2\pi\alpha R_{\text{g}}^2 = 2\pi R_{\text{b}}^2, \tag{3.29}$$

$$\implies R_{\text{g}} = \frac{R_{\text{b}}}{\sqrt{\alpha}} = \sqrt{2}R_{\text{b}}. \tag{3.30}$$

However, note that these integrated cross sections do not depend on the energy of the collision ($\sqrt{s}$) which is not true in nature i.e. we have the integrated cross section as some function of the energy $\sigma(\sqrt{s})$. This also implies in the models above that the radii of the disks must also depend on the energy $R_i(\sqrt{s})$ with $i = b, g$. The function that we will use for both models is $R_i(\sqrt{s}) = a_i \log(b_i\sqrt{s}) + c_i$ where $(a, b, c)_i$ are parameters that are optimized for each i to fit the data (see fig. 7). Note that $R(\sqrt{s})$ is not special and any other function that fits the data can be used. For the grey-disk model, we also introduce the opacity α as a parameter.

3.4 Proton-ion collisions

Combining all previous sections (3.1, 3.2 and 3.3), we can now start the Glauber Monte Carlo simulation. Note that for proton-ion collisions with black disk and grey disk models,

	$y=0$	$y=2$	$y=4$	$y=6$
r	1	1	1	1
$r/3$	0	1	2	3
$r/9$	0	0	1	3
$r/27$	0	0	0	1
N_{dip}	1	2	4	8

Table 1: The approximate behaviour of the dipole evolution (2.15), with the number of dipoles N_{dip} being $\binom{n}{k}$ where n and k are the row and column number respectively.

the number of sub collisions N_{coll} and the number of participating nucleons N_{part} will be the same. A nucleon is considered participating if it has collided with at least one other nucleon. A collision between two nucleons is defined for the black disk model, if the distance between them $r_{\text{b}} < \sqrt{\sigma_{\text{inel}}^{\text{NN}}/\pi} = R_{\text{b}}$ where $\sigma_{\text{inel}}^{\text{pp}} = 42$ mb is the inelastic nucleon-nucleon cross section at $\sqrt{s} = 200$ GeV [9]. For a collision to be counted for the grey disk model, the distance between the two nucleons must be $r_{\text{g}} < R_{\text{g}} = \sqrt{2}R_{\text{b}}$ (assuming $\alpha = 1/2$) and if this is the case, a random uniform number $X \in [0, 1]$ is sampled. If $X < \alpha$, we count it as a collision, otherwise not.

3.5 Dipole-Dipole and γ^*A collisions

Instead of implementing Eq. (2.15) which describes the probability of a dipole evolving in rapidity, we will instead implement a toy model. The evolution of the dipoles then follows the Pascal triangle every two steps in rapidity [4] (see table 1). We start by generating a mother dipole of size $r \propto 1/Q$ according to Eq. (3.21). The dipole is then rotated by a uniform number $\psi \in [0, 2\pi]$ and the evolution begins, keeping one node of the dipole stationary whilst the other rotates by an angle $\alpha = \arccos(1 - 1/2(1/3)^2) = \arccos(17/18)$ around it (from the law of cosines). This creates the first dipole, the second is generated by connecting the rotated node and the original un-rotated node. The first dipole is then discarded and only the two newly generated dipoles are kept. To evolve it further, each of the newly created dipole are then put through the same treatment which then creates 4 new dipoles whilst the originals are discarded according to table 1.

Since we are working with dipoles, we now also make the proton a collection of three dipoles in an equilateral triangle in (x, y, z) with the lengths of each dipole $r \propto 1/3m_p$ where m_p is the mass of the proton. With all of this put together we can then use Eq. (2.13) to calculate f_{ij} for each projectile dipole i which is now the evolved virtual-photon and target dipoles j which is our dipole model of the proton. f_{ij} is then used together with Eqs. (2.11), (2.12) and (2.14) to calculate the integrated total and elastic cross sections of γ^*p for a given virtuality Q and center of mass energy W.

A nucleus can then also be created like in section 3.1 but now instead each proton consists of three dipoles. And in a γ^*A collision, we consider a dipole as collided with another dipole

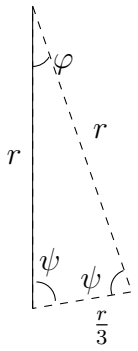

Figure 4: A dipole on the left evolving into 2 other dipoles with lengths r and $r/3$. The angles are $\varphi = \arccos 17/18$ and $\psi = \arccos 1/6$. Note that the original dipole is discarded.

if $f_{ij} > X$ where $X \in [0, 1]$ is a uniform random number. A nucleon is then considered to be participating in the collision if any one of its dipoles has collided.

4 Results and Discussion

In this section, the results from the implementations are presented and discussed.

4.1 Nucleus and impact parameter sampling

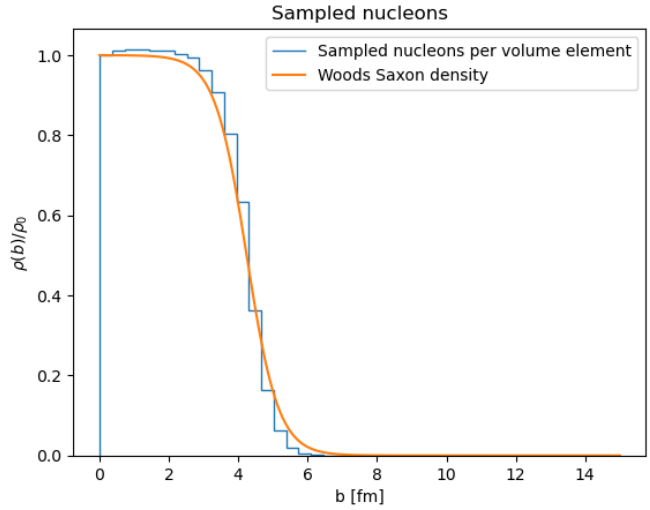

Figure 5: Sampled nucleons per volume element for a copper nucleus ($A = 63$) from the Woods-Saxon distribution compared to the original Woods-Saxon distribution.

The sampled nucleons per volume element with a hard core is shown in figure 5. As we can

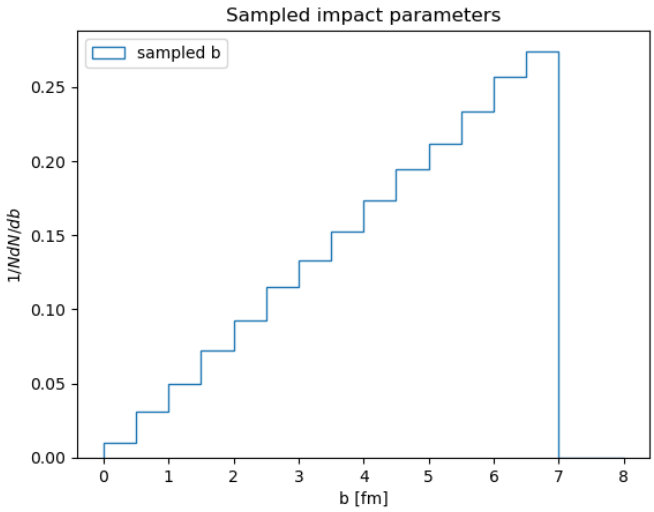

Figure 6: The sampled impact parameter density as according to Eq. (3.21) with $b_{\max} = 7$ fm.

see, the sampled density does not completely match the tail of the Woods-Saxon density. The reason is because of the chosen cut-off for our sampled positions (x, y, z) in section 3.1 has the maximum allowed radius chosen $b = \sqrt{3}R$. The inclusion of the hard core does push the nucleons outwards as they can not clump up at the center, however not enough for it to be visible.

Another method to encompass the whole WS was tried but was unsuccessful in implementation. This method implemented a custom function $g(r)$ (ex. a piece-wise constant and exponential) instead of the box $X \in [0, 1]$ with constrained coordinates, which would follow the WS and also converge (note that $g(r)$ must be larger than WS for all r). We would then sample an r according to $g(r)$ exactly like in section 3.2 and set a new value $y = Xg(r)$ ($X \in [0, 1]$ is a uniform random number) and if $\text{WS}(r) > y$ we accept the position r for the nucleon (would also need to include a hard core repulsion afterwards) otherwise go back and sample a new r from $g(r)$. This method would be more accurate as it would sample from the whole distribution and also potentially faster depending on how close $g(r)$ is to the WS.

In figure 6 we see the density of sampled impact parameters b for the projectiles. As we can see the density of sampled impact parameters is indeed linear with with the chosen sharp cutoff at $b = 7$ fm. The reason for having the cutoff here is that very few nucleons are further away from the center of the nucleus. This can be seen in figure 10 where the average number of participating nucleons for both the black and grey disk models are close to zero at $b > 6$ fm.

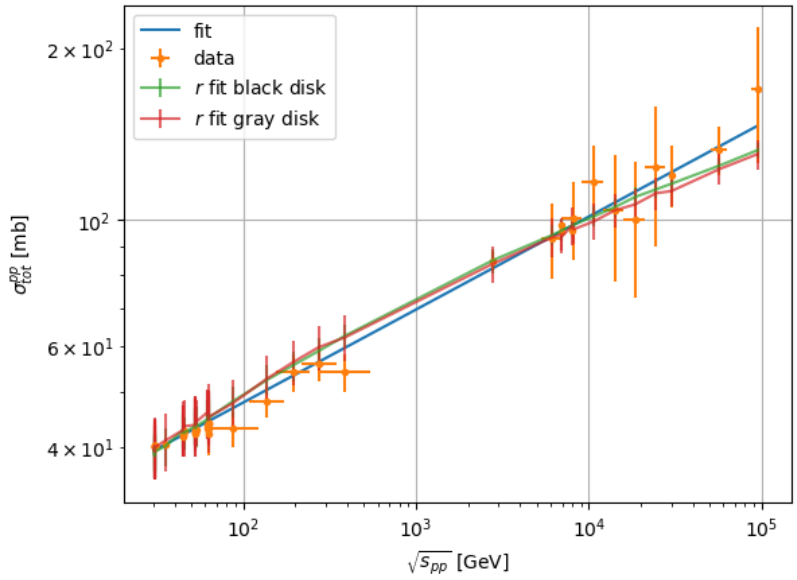

Figure 7: Total integrated cross section for grey disk and black disk model in pp collision as a function of $\sqrt{s}$ compared to the data and a fit of the data [10] $\sigma_{tot}^{pp} = \exp(a \log(\sqrt{s})) + b$ with $a = 0.16$ and $b = 3.12$.

4.2 Proton-proton collisions

In figures 7 and 8 we see the data for the integrated total and elastic cross sections at different $\sqrt{s}$. The radius and opacity (grey-disk only) are fit according to the data separately in figure 7 as described in section 3.3 and the same parameters (see table 2) are then used to calculate the elastic cross section in figure 8. As can be seen from figure 7, the black and grey disks follow each other, both falling off at the higher energies compared to data. This is most likely due to how $R(\sqrt{s})$ is chosen to be a logarithmic function. Other functions where tested such as various polynomial functions, however they were unsuccessful in fitting the data.

Now comparing the two methods to the elastic cross section we see that both of the two models fail at following the data with the grey disk being slightly more accurate. Whilst there is not really much that can be done for the black disk model, there are ways to improve the grey-disk model. One way of doing this might be to limit the fit to a smaller opacity α or also instead of just having $R(\sqrt{s})$, have $\alpha(\sqrt{s})$ as an increasing function too. We know that the proton, due to confinement, gets "blacker" (i.e larger α and hence larger $\sigma_{\text{el}}/\sigma_{\text{tot}}$) with $\sqrt{s}$ and hence having α increasing with $\sqrt{s}$ would make sense. One could also, with a better method for fitting, make the grey disk model fitted according to both the total and elastic integrated cross sections and not just one or the other as is done here.

Model	a [fm]	b [GeV^{-1}]	c [fm]	α
Black Disk	0.08	1.05	0.50	
Grey Disk	0.11	0.97	0.74	0.50

Table 2: Fitted parameters to the total integrated cross section of the black and grey disk models with the radius $R = a_i \log(b_i\sqrt{s}) + c_i$.

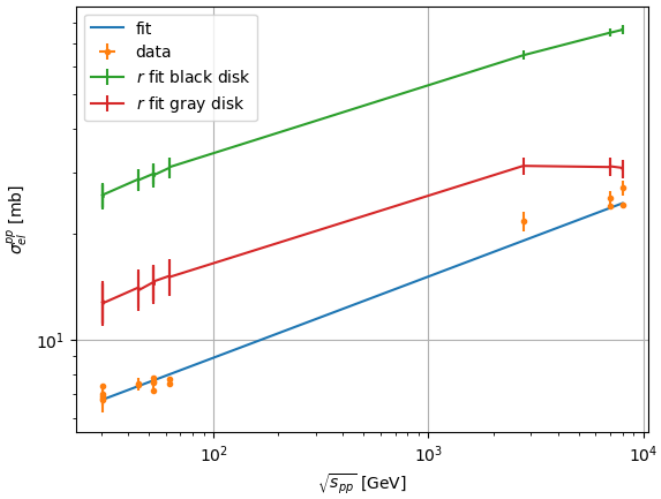

Figure 8: Integrated elastic cross section for the grey disk and black disk models in a pp collision as a function of $\sqrt{s}$ compared to data [10] and a regular fit of the data $\sigma_{el}^{pp} = \exp(a\log(\sqrt{s})) + b$ with $a = 0.23$ and $b = 1.12$.

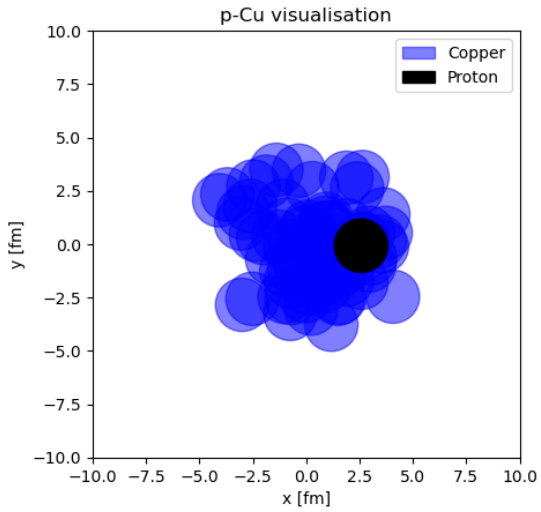

Figure 9: Visualisation of p-Cu collision in the xy plane where each blue circle represents a nucleon inside the target copper nucleus and the black circle represents the projectile proton.

4.3 Proton-ion collision

In figure 9 we see the visualisation of a 2D slice for the p-Cu collision with the protons radius $R = R_b$ (R_b being the black disk radius). The average number of participants as a function of impact parameter can be seen in figure 10. As we can see, the black and grey disk models are quite similar to each other, however note that the grey disk is slightly broader than the black disk. This is due to the overall radius of the grey disk being larger and the fact that even if two nucleons overlap, they are not guaranteed to collide. The disk being larger means that we will have more collisions at low centrality (large b) but due to it having an opacity, the number of collisions at high to mid centrality goes down. We also see that the standard deviation for the grey disk is larger due to it including an opacity parameter.

In figure 11 we see the probability of having a certain number of participating nucleons N_{part} in a proton-copper collision. As we can see, there is not a lot of difference in the probabilities for the black and grey disks. However we do see that the grey disk is a little bit broader with more probability of having no and more collisions than the black disk model. This is because of the opacity (sometimes the projectile doesn't hit) and the radius of the grey disk is larger.

4.4 Dipole-dipole collisions

Moving on to the dipole-dipole model, in figure 12 we see the number of participating nucleons density in a virtual-photon-gold collision ($A = 197$). The probability density

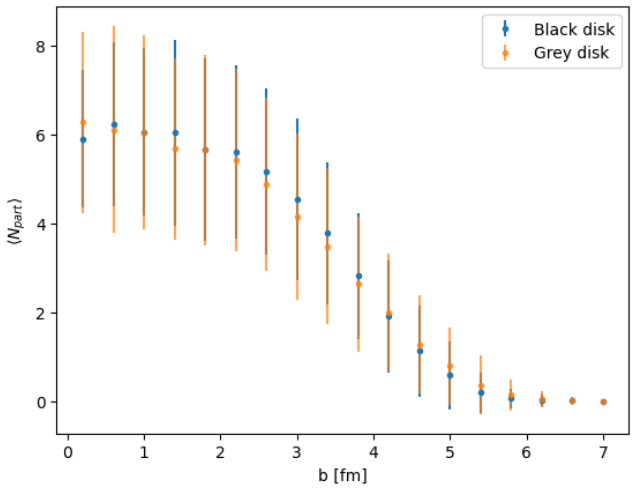

Figure 10: The average number of participating nucleons $\langle N_{part} \rangle$ for proton-copper as a function of the impact parameter b. The error-bars represent 1 standard deviation.

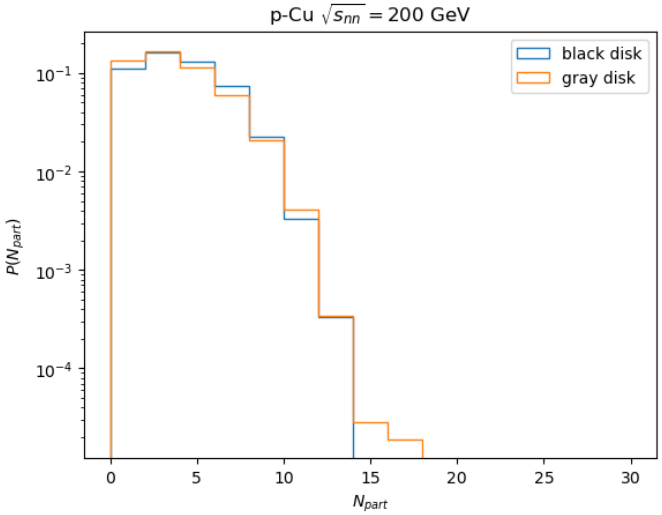

Figure 11: The probability of having N_{part} participating nucleons in the black and grey disk model for proton-copper $A = 63$ at $\sqrt{s} = 200$ GeV.

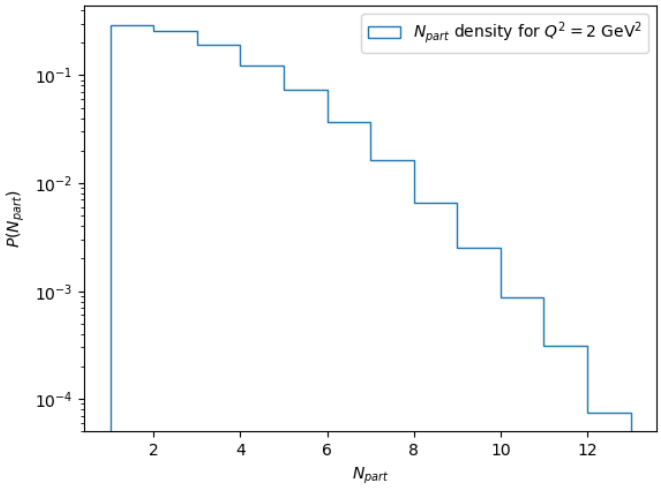

Figure 12: The probability of having N_{part} participating nucleons in a $\gamma^* A$ (A=197) collision at $Q^2 = 2$ GeV^2 and $W^2 = 5000$ GeV^2.

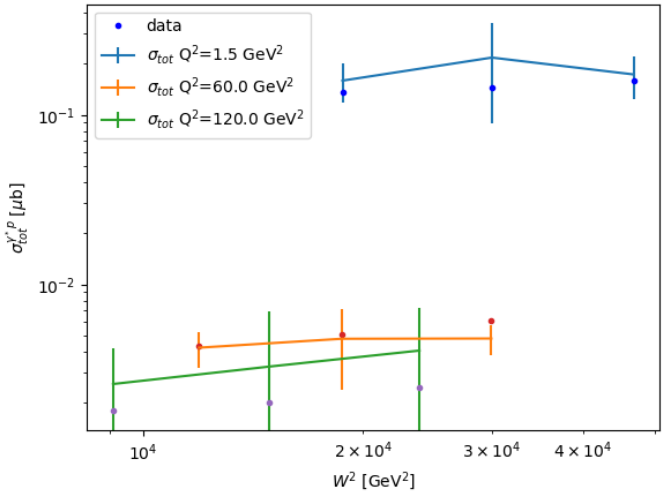

Figure 13: Total integrated cross section in a γ^*p collision for different values of Q^2 for the pascal model compared to data [11].

of the number of participating nucleons N_{part} decreases slowly at small N_{part} and more rapidly at larger N_{part} in the log plot. This does not represent what has been observed in [5] (PYTHIA 8) which uses a more "physical" dipole model stemming from Eq. (2.15) (instead of the toy model) where the probability decreases rapidly for the first few participants and then tapers off. The key differences between the two models are that the dipoles can fluctuate in size instead of being fixed as in they are in the Pascal model and that the evolution of the dipole is probabilistic which means that at fixed y we do not have a fixed number of dipoles. Then one way to improve the Pascal model (or see if this is why they differ) could be to allow the dipoles to fluctuate. For example, the steps in rapidity could fluctuate for each virtual-photon and the dipole size could also be allowed to fluctuate in size.

In figure 13, we see the total integrated cross sections for γ^*p in our implemented dipole model. As we can see, the model follows the data reasonably well by taking the mother dipole $r = 5.068z/Q$ fm with $z = 0.0005$ being a fitting parameter, Q in GeV and where 5.068 is the conversion factor from GeV^{-1} to fm. Note that in this implementation, only the virtual-photon is allowed to evolve. This could be improved upon by allowing for the protons to evolve too with W^2 as we know that the proton gets blacker with larger center of mass energies. So in figure 13 we see that as we increase the virtuality of the photon, the cross section gets smaller. This is because the size of the mother dipole decreases. According to Eq. (2.13), for any two dipoles, if the dipoles have a larger size (i.e. smaller Q), the probability to have a larger f_{ij} increases. And an increase in f_{ij} then leads to $T(\mathbf{b})$ being larger according to Eq. (2.14) and hence also the total integrated cross section for the dipole model increases (see Eq. (2.12)). Now if the center of mass energy W would increase, the rapidity y would too. An increase in y for our model means potentially more dipoles according to table 1 which would lead to $\sum_{ij} f_{ij}$ being larger and hence the total integrated cross section increases.

5 Conclusion and outlook

As we have seen, the models that have been implemented here do follow the data to a certain extent and we have seen how the centrality of the collision affects the number of participating nucleons in both proton-ion and virtual-photon-ion collisions. The grey and black disk models for proton-proton collisions did well following data for total integrated cross section but not for the elastic integrated cross section. For the dipole-dipole toy model, it somewhat follows the data for the total integrated cross section for virtual-photon-proton collisions. There are plenty of ways to improve and optimize on these models used. The grey disk model can be fit to both the total and elastic integrated cross sections instead of just the total together with the opacity as a function of the center of mass energy $\alpha(\sqrt{s})$. The nucleons can be sampled from the Woods-Saxon distribution with a more precise and efficient method as stated in section 4.1 and the dipole-dipole model could include fluctuating dipole sizes and evolving protons.

But in conclusion, we have seen that from optical theorem and the Good-Walker formalism that we can build models that can be fitted and predict integrated cross sections in both proton-proton and virtual-photon-proton collisions.

References

[1] E. D. Bloom, D. H. Coward, H. DeStaebler, J. Drees, G. Miller, L. W. Mo, R. E. Taylor, M. Breidenbach, J. I. Friedman, G. C. Hartmann, and H. W. Kendall. High-energy inelastic $e - p$ scattering at 6° and 10°. *Phys. Rev. Lett.*, 23:930–934, Oct 1969.

[2] Christian Bierlich, Smita Chakraborty, Nishita Desai, Leif Gellersen, Ilkka Helenius, Philip Ilten, Leif Lönnblad, Stephen Mrenna, Stefan Prestel, Christian T. Preuss, Torbjörn Sjöstrand, Peter Skands, Marius Utheim, and Rob Verheyen. A comprehensive guide to the physics and usage of pythia 8.3, 2022.

[3] G. Marchesini, B.R. Webber, G. Abbiendi, I.G. Knowles, M.H. Seymour, and L. Stanco. Herwig 5.1 - a monte carlo event generator for simulating hadron emission reactions with interfering gluons. *Computer Physics Communications*, 67(3):465–508, 1992.

[4] Christian Bierlich, Gösta Gustafson, and Leif Lönnblad. Diffractive and non-diffractive wounded nucleons and final states in pA collisions. *JHEP*, 10:139, 2016.

[5] Christian Bierlich and Christine O. Rasmussen. Dipole evolution: perspectives for collectivity and γ^*A collisions. *JHEP*, 10:026, 2019.

[6] Maciej Rybczyński, Grzegorz Stefanek, Wojciech Broniowski, and Piotr Bożek. GLISSANDO 2: GLauber initial-state simulation AND mOre..., ver. 2. *Computer Physics Communications*, 185(6):1759–1772, jun 2014.

[7] F. Nemes. The totem experiment at the lhc and its physics results. *Nuclear Physics B - Proceedings Supplements*, 245:275–282, 2013. The Proceedings of the 7th Joint International Hadron Structure'13 Conference.

[8] J. Adam et al. Results on total and elastic cross sections in proton–proton collisions at s=200 gev. *Physics Letters B*, 808:135663, 2020.

[9] Wojciech Broniowski, Maciej Rybczyński, and Piotr Bożek. GLISSANDO: GLauber initial-state simulation AND mOre.... *Computer Physics Communications*, 180(1):69–83, jan 2009.

[10] R. L. Workman et al. Review of Particle Physics. *PTEP*, 2022:083C01, 2022.

[11] C. Adloff et al. and. Deep-inelastic inclusive ep scattering at low x and a determination of α_s. *The European Physical Journal C*, 21(1):33–61, jun 2001.